Quantitative Morphometry of Mammalian Sperm Head to Find High Fertilizing Ability Indicators

By
Mashiko Daisuke

Chapter1: Introduction and Aim of the Thesis

Fertilization: a sperm's journey to and interaction with the oocyte

When sperm encounter with the egg which is gradually released from the follicle (Lousse, Donnez, 2008), fertilization occurs. Ejaculated sperm moves from the vagina to the uterus, the oviduct and penetrates the zona pellucida. Finally, sperm reaches the surface of the egg (Fig.1-1). The group of sperm (spermatozoa) in uterus/oviduct have a higher fertilization rate than those collected just after ejaculation [Sztein et al., 2000; Cohen et al., 1974; Fischer et al., 1981; Siddiquey et al., 1982]. What features do the spermatozoa with high fertilizing ability have?

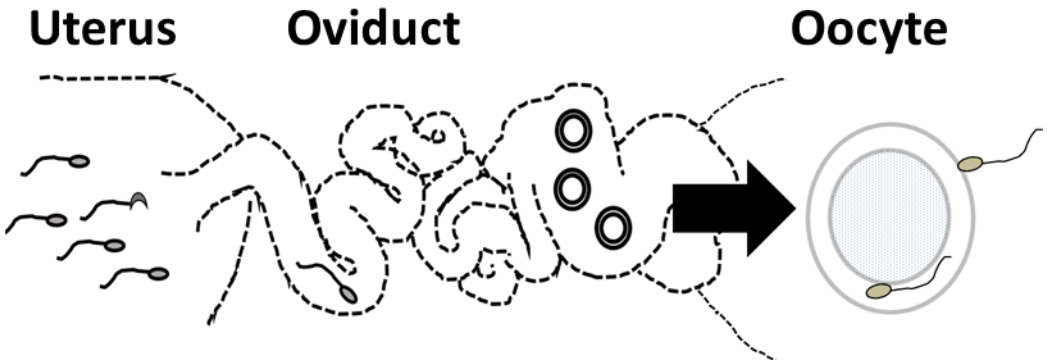

Figure. 1-1 The schematic diagram of sperm journey in the female reproductive tract.
From left to right, uterus, oviduct, and oocyte are shown.

Motility, morphology, and number of sperm are equally contributed to fertilizing ability

In order to evaluate the fertilizing ability, ratio of motility (motile/total spermatozoa),

ratio of normal morphology(normal/total spermatozoa), and number [World Health Organization, 2010], have been used [Jouannet et. al., 1988; Toner et al., 1995; Eggert-Kruse et al., 1996; Coetzee et al., 1998; Menkveld et al., 1990; Van Waart et al., 2001; Garrett et al., 2003; Liu et al., 2003]. According to a large cohort study (765 infertile couples and 696 fertile couples), the defects of motility, morphology and the number are additively and equally contributed to the failure of fertilization. [Guzick et al., 2001; When each factor of the spermatozoa in semen has the defect, the infertile risk of morphology will 2.9 times increase, that of motility will 2.5 times increase and that of the number will 2.2 times increase].

There is no research on morphology for choosing a good sperm from many spermatozoa.

One feature that can be assessed in a low-cost, high-throughput manner is sperm head morphology, which is affected by defects in nuclear structures (DNA [Gandini et al., 2000], chromosomes [Lee et al., 1996], chromatin [Dadoune et al., 1988; Devillard et al., 2002; Martin et al., 2003]). Most early studies on sperm fertilization indicators distinguished normal sperm from abnormal sperm, which failed to fertilize or resulted in spontaneously aborted embryos [Fredricsson et al., 1977; Menkveld et al., 1990; Menkveld et al., 1991; Liu et al., 1992; Vilyana et al., 2017; They found that the normal sperm have oval morphology.]. While research had been conducted to eliminate abnormal spermatozoa,, it would be beneficial to distinguish spermatozoa with a better chance of fertilization among the population of normal sperm. For example, selection of good sperm morphology is beneficial when injecting a single sperm into an ovum in the medical therapy known as intracytoplasmic sperm injection (ICSI, Fig. 1-2, Palermo et

al., 1992), ICSI is an alternative when *in vitro* fertilization (IVF; Fig. 1-2) does not work to resolve male infertility. It is unclear whether the spermatozoa with high fertilizing ability exists in normal spermatozoa or not, because normal sperm indicators that are quantitatively correlated with the success of fertilization have not been well studied.

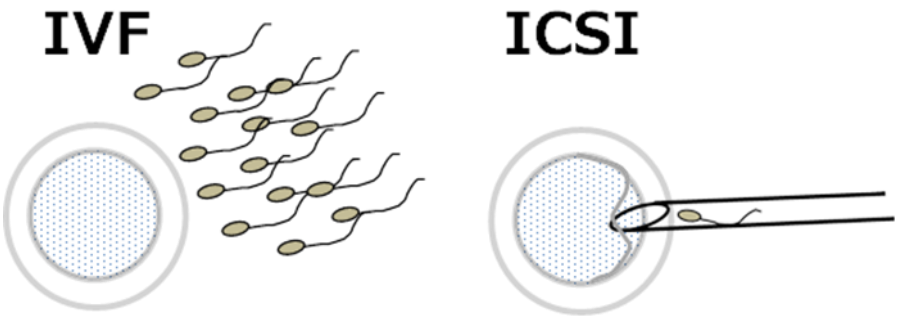

Figure. 1-2 In vitro fertilization (IVF) and intracytoplasmic sperm injection (ICSI). IVF is a method of sprinkling motile spermatozoa on oocytes. IVF is often used for expressing fertilizing ability of spermatozoa with fertilization ratio (the numbers of zygote / the numbers of oocyte). ICSI is a method that selected a single sperm is injected to an oocyte. ICSI is an alternative when IVF does not work.

Heterogeneity of normal sperm head morphology affects fertilizing ability.

Even normal spermatozoa in semen are morphologically heterogeneous in their head shape in mammals [Severa et al., 2010; Ramón et al., 2014]; human normal sperm morphologies have a range of 2.5–3.2 μm in width and 3.7–4.7 μm in length based on the WHO manual [World Health Organization, 2010]. Interestingly, semen containing an abundance of normal spermatozoa with elongated heads show higher fertilization ratio than that with rounded heads [Ramón et al., 2014]. This comparative

morphology of sperm achieved some success as it was used to arbitrarily classify continuous variations of sperm head morphologies into several discrete categories which correlate fertilization ratio.

How to quantify the morphological information

To distinguish normal sperm head morphologies, it has been unclear whether conventionally used indicators such as length, width, and angle are optimal (Fig.1-3). Moreover, they could underestimate complex head contours by merely measuring distances between subjectively selected points. Geometric morphometrics combining multivariate quantification of contour with systematic extraction of indicators have been developed to circumvent such shortcomings, and this analysis has been applied to evaluate morphological heterogeneities in mice [Oka et al., 2007], bovine [Ostermeier et al., 2001], stallion [Severa et al., 2001], and human [Utsuno et al., 2013] sperm. The Elliptic Fourier descriptor (EFD) is a representative method to quantify any contour (closed curve) using multiple ellipses [Severa et al., 2010, Kuhl et al., 1982; Iwata et al., 2002; Utsuno et al., 2013; Beletti et al., 2005]. Principal component analysis (PCA) can provide the optimal indicators to maximize variance among data (head contour of spermatozoa) and compress multivariate information into lower dimensions while retaining most of the original information. EFD and PCA are tools suitable for measuring sperm morphology without decreasing the amount of information.

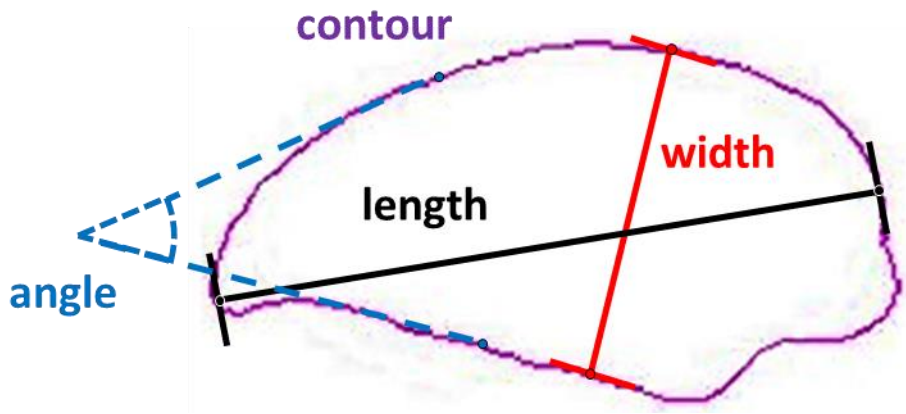

Figure 1-3. Conventional method of sperm head shape quantification

Parameters such as length, width, and angle are usually obtained by intuitively selecting points and measuring them. However, these parameters have a risk to underestimate the complex shape of sperm head contour.

Quantitative morphometry to explore indicators of fertilization success

There are a few studies that show the correlation between sperm morphology and its functions using EFDs and PCA. W. Yi et al., 1998 had succeeded to distinguish abnormal from normal spermatozoa by EFDs and PCA. Utsuno et al. 2013 showed the correlation between DNA fragmentation (damage) and sperm head morphology using EFDs and PCA. Utsuno et al. 2014 revealed the correlation between protamine deficiencies and sperm head morphology. These studies show that measuring head morphology is effective to avoid choosing the DNA fragmented spermatozoa when we perform ICSI (DNA fragmented sperm cause the abnormal embryonic development [Tamburrino et al., 2012]). However, good sperm morphology has not been searched among normal spermatozoa. In order to find the morphological indicators that correlate

with the success of fertilization, it is necessary to quantitatively compare multiple normal spermatozoa with different fertilizing ability using the combined method of EFDs and PCA. If this method would distinguish sperm with high fertilizing ability from sperm with low fertilizing ability, it would be advantageous to explore the fertilization indicators. The pipeline integrating geometric morphometrics with comparative morphology among normal spermatozoa with different fertilizability could objectively identify morphological indicators that correlate with the success of fertilization.

The application of morphological indicators: Does the morphology change during sperm maturation process?

The morphological indicator can be used not only for choosing good sperm but also for finding out where morphological changes will occur. In the epididymis, sperm motility is acquired (Fig. 1-4A), and this change in sperm is called sperm maturation. The midpiece of sperm has rigidity in epididymis caput but loses rigidity in epididymis corpus (Fig. 1-4B and 1-4C; Miyata et al., 2015), and they show that the PPP3CC, the protein giving the flexibility to sperm in epididymis caput, is important for fertilization (Miyata et al., 2015). Regardless of the progress of sperm motility research, the morphology of spermatozoa in epididymis has not been described. By finding where the morphology changes, we may find the genes which show the changes of expression in that place.

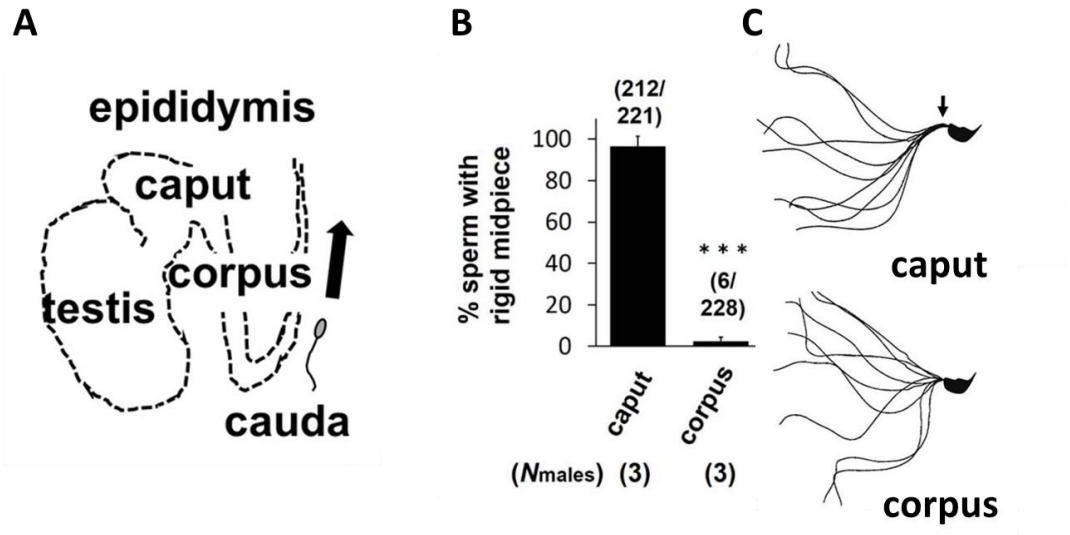

Figure. 1-4 The sperm maturation is caused in the epididymis.
(A)The schematic diagram of epididymis caput, corpus, cauda (B, C) During sperm maturation, midpiece of sperm will loss the rigidity (Miyata et al., 2015).

The aim of the thesis: To find the fertilization success indicators

To develop a pipeline that can determine indicators for high fertilizability, I examine mice (Chapter 2: Mouse Spermatozoa with Higher Fertilization Rates Have Thinner Nuclei) and human (Chapter 3: Application of Quantification Procedure to Human Sperm) spermatozoa. Mice spermatozoa are a valuable model system because spermatozoa having known differences in fertilization rates (i.e., collection sites of spermatozoa and mouse strains) are available. The hybrid BDF1 strain (F1 of inbred B6N × DBA/2) has higher fertilization ability than the inbred C57BL/6N (B6N) strain [Sztein et al., 2000]. Spermatozoa that reach close proximity to the egg (i.e., those in the cervical canal and in oviduct) are known to have higher fertilizability than those collected just after ejaculation [Sztein et al., 2000; Cohen et al., 1974; Fischer et al., 1981; Siddiquey et al., 1982]. Therefore, I applied geometric morphometrics to analyze

sperm head contours within a population and between mouse strains and collection sites of spermatozoa. I also compared the human sperm head morphology between fertile male and infertile male to identify morphological indicators that correlate with the success of fertilization.

Chapter2: Mouse Spermatozoa with Higher Fertilization Rates Have Thinner Nuclei

Abstract

Background. Although spermatozoa with normal morphology have been assumed to have uniform fertilization ability, recent data show that even normal spermatozoa have considerable variation in their head shape which is associated with differences in fertilization ability. Appropriate quantitative indicators for good sperm morphology, however, remain unidentified.

Methods. Therefore, in an effort to identify such an indicator, I compared the nuclear contour of normal mouse spermatozoa by quantitative multivariate analysis using EFDs combined with PCA. The spermatozoa were obtained from different strains and collection sites which have been shown to be associated with different fertilization abilities.

Results. I found that the head was 5.7% thinner in spermatozoa from the B6D2F1 (BDF1) strain, known to have a higher fertilization rate, than in those from the C57BL/6N (B6N) strain, which has a lower fertilization rate. Moreover, zona-penetrated spermatozoa in the perivitelline space consistently had 5.4% thinner heads than those isolated from the epididymis before ejaculation. The aspect ratio, which represents the sperm head thinness, uniquely distinguished these sperm populations, confirming its validity as a morphological indicator.

Discussion. Because we are able to measure the aspect ratio of human spermatozoa, this

unique morphometric indicator might be applicable to compare normal spermatozoa among multiple patients, which will greatly facilitate and enhance current reproductive technologies.

Materials and Methods

Animals

All animal experiments were approved by the Animal Care and Use Committee at the Research Institute for Microbial Diseases at Osaka University [permit number: 2589, 3514]. C57BL/6N (B6N) and BDF1 mice (12 weeks old) were obtained from SLC (Japan SLC, Inc. Shizuoka, JP).

Abnormality test

Based on the morphological criteria for sperm abnormality that were described previously [Touré et al., 2004; Wyrobek&Bruce, 1975; Bruce et al., 1974; Watanabe 1991], I defined abnormal sperm as morphology outliers that showed a PC1 score > 0.55 and largely lacked the hook-shaped heads common to most sperm.

In vitro fertilization and spermatozoon collection

Females (N = 16) were superovulated by injecting 5 IU of pregnant mare serum gonadotropin (PMSG, ASKA Pharmaceutical Co., Ltd. Tokyo, JP), and then, 5 IU of human chorionic gonadotropin (HCG, ASKA Pharmaceutical Co., Ltd. Tokyo, JP) 48 h after the PMSG injection. The ovulated oocytes were collected from the oviducts 14 h after the HCG injection. Cumulus-enclosed oocytes were placed in 100 μl drops of TYH medium [Toyoda et al., 1971] covered with paraffin oil (Nacalai Tesque, Kyoto, JP). The spermatozoa collected by mechanically-dissecting cauda epididymides (N = 5) were placed in 100 μl drop of TYH medium. After a 2-h incubation, the sperm suspension in TYH was added to the TYH drop containing eggs at a concentration of 5 × 10^5 sperm/ml. After 2-8 h co-insemination of the spermatozoa and oocytes, the zona-

bound spermatozoa were carefully removed using a holding needle. Because of the technical difficulty associated with collecting sperm in the zona pellucida of an oocyte by manipulation [Inoue et al., 2011], I obtained zona-penetrated spermatozoa using acidic Tyrode's solution after *in vitro* fertilization. Acidic Tyrode's solution treatment did not affect the sperm head aspect ratio. Zona pellucida was removed from the oocyte in 20 μl acidic Tyrode's solution drops on a glass slide. The spermatozoa attached to the egg surface were removed by pipetting, and subsequently, the eggs were removed from the drops.

Epididymal spermatozoa were collected by dissecting the caput, corpus and cauda epididymides (N = 5 for each experiment) and placed into 400 μl phosphate buffered saline (PBS). Spermatozoa were collected from the oviduct and uterus by flushing out these structures with PBS 4 h after coitus.

Spermatozoon imaging and analysis

The spermatozoa were coated onto a glass slide (Matsunami Glass, Osaka, JP) and stained with 65 μM Hoechst 33342 (Life Technologies, Carlsbad, CA). The slides were viewed using an Olympus IX-70 fluorescence microscope with a 10× eyepiece and 100× objective lens (Numerical aperture is 1.4). The sperm head contours were derived from image binarization using the discriminant analysis method [Otsu 1979] in OpenCV (available also in ImageJ, http://imagej.nih.gov/ij/), which was customized using C programing language.

Elliptic Fourier descriptors and principal component analysis

Each sperm head was transferred to EFDs with two-dimensional coordinates given by:

$$\begin{cases} X(t) = \sum_{n=1}^{N} \left(a_n \cos\frac{2n\pi t}{T} + b_n \sin\frac{2n\pi t}{T} \right) \\ Y(t) = \sum_{n=1}^{N} \left(c_n \cos\frac{2n\pi t}{T} + d_n \sin\frac{2n\pi t}{T} \right) \end{cases} \quad (1)$$

where n, N, t, and T denoted the harmonic number, the maximum harmonic number, the displacement along the contour, and the total displacement, respectively. At $N = 1$, ($X(t)$, $Y(t)$) represented an ellipse. I set a_n, b_n, c_n, and d_n as parameters of the PCs. The number of coefficients was provided as $4N$-3 because normalization was carried out for the size and angle of the first harmonic ellipse with $a_1 = 1$, $b_1 = 0$, and $c_1 = 0$. The variable d_1 denoted the aspect ratio. I approximated the contours of the heads of spermatozoa up to 20 ellipses (N = 20), and I performed the PCA on 77 parameters and the data reconstruction on the PC scores using SHAPE (http://lbm.ab.a.u-tokyo.ac.jp/~iwata/shape/index.html) [Iwata et al., 2000].

Calculation of contribution rate

The variance of each principal component is denoted as l_1 to l_N. The contribution ratio of the Nth component can be expressed by $\frac{l_N}{\sum_{t=1}^{N} l_t} \times 100$ (%).

Statistics

Kolmogorov-Smirnov test, Shapiro-Wilk test for checking normality, *F*-tests for checking homoscedasticity, *t*-tests and Steel-Dwass tests were performed using custom R programs. A *P*-value > 0.05 was considered not significant (n.s.), whereas *P*-values < 0.05 (*), < 0.01 (**), and < 0.001 (***) were considered significant.

Results

EFD and PCA revealed sperm head aspect ratio as a unique fertility indicator.

In order to compare zona penetrated spermatozoa and ejaculated sperm, I focused on the contour of the nucleus, which does not change by spontaneous acrosome reaction (See Figure S1-C). To quantify the variations in sperm head morphology, I first collected spermatozoa (n = 179) from dissected B6N male cauda epididymides (Fig. 2-1A) and tracked the sperm head contour (Fig. 2-1B) by taking the pictures of each spermatozoon nucleus (Fig. S2). The tracked contour was sequentially inputted into a quantitative descriptor EFD method (see "Image analysis" and “Elliptic Fourier descriptors and principal component analysis” in Materials and Methods; Fig. S3). To extract normal sperm characteristics, I subsequently performed PCA after subtracting out the abnormal spermatozoa (see "Abnormality test" in Materials and Methods; Fig. S4. Applying this protocol, I quantified the variation in head morphology of normal spermatozoa, as optimally separated into multiple principal components (PCs; Fig. S5), among B6N (n = 170, Fig. 2-2A) and BDF1 spermatozoa (n = 163, Fig. 2-2B). PC1 of the B6N spermatozoa highlighted variations in width (Figs. 2-2A and S5, whereas PC2 highlighted variations in the hook shape of the tip (Fig. S5).

To identify the PCs that correlate with fertilization ability, I focused on PC1, PC2, and PC3, whose contribution rates were above 10% for B6N normal sperm (49.8%, 19.3%, and 12.7%, respectively; Fig. S4). First, I identified the PCs that distinguished the BDF1 from the B6N spermatozoa and the epididymis-isolated from the zona-penetrated B6N spermatozoa (see "*In vitro* fertilization" in Materials and Methods). Regarding mouse strain, the BDF1 and B6N spermatozoa collected from the cauda epididymis showed differences in PC1, PC2, and PC3 (Figs. 2-2C and S5).

However, regarding collection sites of spermatozoa, the epididymis-isolated and zona-penetrated B6N spermatozoa differed in PC1, but not in PC2 or PC3 (Figs. 2-2C and S6). Thus, PC1 uniquely distinguished spermatozoa between mouse strains and between collection sites of spermatozoa.

Next, I tried to identify the morphological parameters contributing to PC1. The width of the sperm head, defined as the longest part of the head perpendicular to its length, seemed to be highlighted in PC1 (Fig. 2-2A), but the error in width measurement was large. On the other hand, the major and minor axes of the ellipse representing the lowest mode of the sperm head EFD were almost precisely overlapped with the antero-posterior (length) and dorso-ventral (width) axes of the sperm head, respectively (Figs. 2-3A and S7A). Thus, I used these major and minor axes to calculate the aspect ratios (minor axis divided by the major axis, equivalent to d_1 in Eq. (1); Fig. 2-3A). I found that the sperm head aspect ratios of BDF1 caudal spermatozoa (n = 330) were reduced compared with those of B6N spermatozoa (Fig. 2-3B; n = 298, N = 5; one-tailed *t*-test, $P = 2.1 \times 10^{-16}$), whereas the sperm head areas were not significantly different between the two groups (Fig. S8A, B; n = 687 for BDF1; n = 465 for B6N; two-tailed *t*-test, $P = 0.53$). Moreover, the factor loading (correlation) of the aspect ratio on PC1, which was proportional to the correlation coefficient with PC1, was more than 2-fold higher than that of any of the other parameters of the EFDs (x-coordinate in Fig. 2-3C). Thus, by combining PCA and EFDs, I established a quantitative evaluation pipeline of multi-dimensional morphological variation, and using this pipeline, I identified a low aspect ratio, i.e., a thin sperm head, as a unique and optimal morphological indicator of the fertilization ability of spermatozoa.

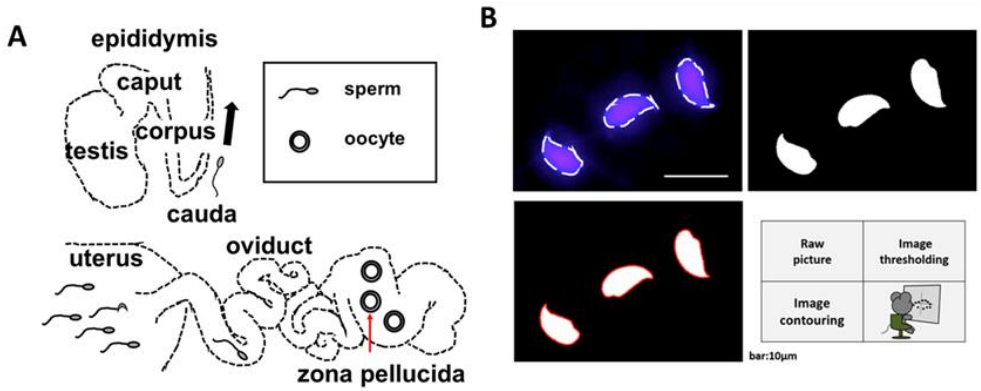

Figure. 2-1 Schematic diagrams illustrate the methods of spermatozoon isolation and sperm head contour extraction.

(A) The male (upper) and female (lower) reproductive tracts. Spermatozoa were collected from the epididymis of males or the oviducts or uteri of females. Zona-penetrated spermatozoa were isolated following *in vitro* fertilization. The red arrow shows the zona pellucida. **(B)** The shapes of the sperm heads were visualized using Hoechst 33342 to stain the nuclei (upper left panel). Image binarization (upper right) and extraction of the contours (lower left) were subsequently performed.

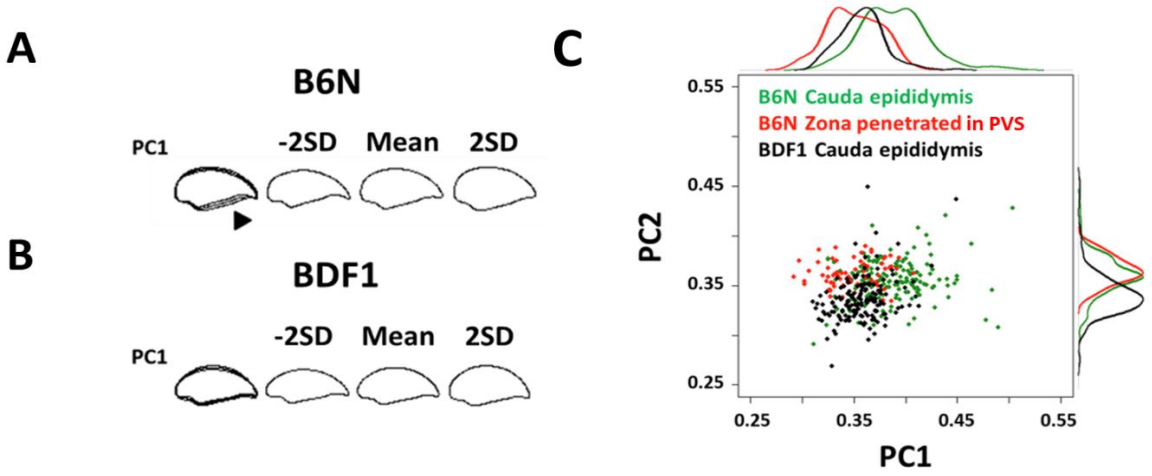

Figure. 2-2 The first principal component distinguished variation in normal spermatozoa among strains and fertilization stages.

From left to right, the overlapping, -2 standard deviation (SD), mean, and +2 SD sperm head contours of the first principal component (PC1) are shown from **(A)** B6N and **(B)** BDF1 mouse epididymis-isolated spermatozoa. The arrowhead shows the region of increased variation. **(C)** A scatter plot and the associated density curves (outside of the x- and y-axis) of the PC scores of B6N zona-penetrated spermatozoa (red), and B6N (green) and BDF1 (black) cauda epididymis-isolated spermatozoa. The distribution of each group partially overlapped at PC1 = 0.3–0.4. The eigenvectors of the PCs were derived from the principal component analysis (PCA) of B6N epididymis-isolated spermatozoa.

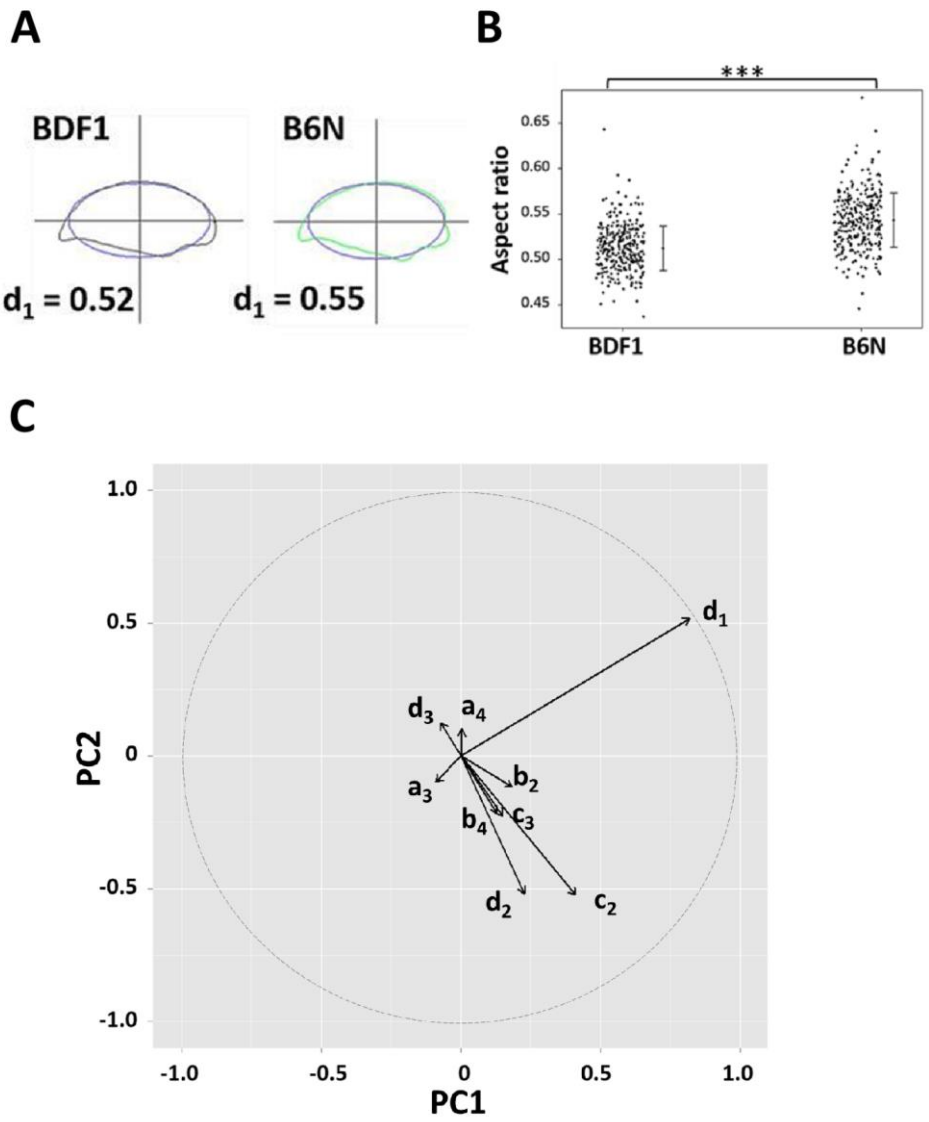

Figure. 2-3 The sperm head aspect ratio was the largest contributor to the first principal component.

(A) Representative sperm head shapes of BDF1 (gray) and B6N (green) epididymis-isolated spermatozoa are shown with the overlapping ellipse (blue) used to calculate population mean of the aspect ratio (d_1 in Eq. (1)). **(B)** A dot plot shows the aspect ratio of the heads from BDF1 and B6N spermatozoa. The error bars denote the standard deviation (SD). **(C)** The arrows show the eigenvectors of the PC projected into PC1-PC2 space, whose length (the square-root of the sum of the square of the factor loadings of PC1 and PC2) is greater than 0.1, and where the dashed circle denotes the norm of the eigenvector = 1.

The sperm head aspect ratio decreased during the progression of fertilization.

I next compared the sperm head (nucleous) aspect ratio from cauda epididymis-isolated B6N spermatozoa (n = 118, green in Fig. 2-4) with zona-penetrated B6N spermatozoa isolated from the perivitelline space (PVS) (n = 133, red in Fig. 2-4 and Fig. S9). The sperm head aspect ratio of zona penetrated spermatozoa was significantly smaller than that of cauda spermatozoa (Fig. 2-4; unpaired, one-tailed *t*-test, $P = 2.2 \times 10^{-16}$), further confirming the validity of the sperm head aspect ratio as a fertilization indicator. Moreover, the B6N zona penetrated spermatozoa had an aspect ratio that was similar to that of BDF1 cauda epididymis-isolated spermatozoa (Fig. 2-4, Kolmogorov-Smirnov test, $P = 0.57$), which have a higher fertilization rate than B6N epididymis-isolated spermatozoa. Importantly, the mean aspect ratio of spermatozoa decreased throughout the progression of fertilization, and it was consistently negatively correlated with the fertilization ability of the spermatozoa. To investigate whether the sperm head aspect ratio decreased during sperm maturation in male mice prior to ejaculation, I collected spermatozoa from each region of the epididymis, including the caput, corpus, and cauda (Fig. 2-4A). The mean aspect ratio of spermatozoa from the caput (n = 69, purple box in Fig. 2-4) was 3.0% larger than that from the corpus (n = 85, sky blue in Fig. 2-4; Steel-Dwass test, $P = 0.01$) and 2.6% larger than that from the cauda (n = 118, green in Fig. 2-4; Steel-Dwass test, $P = 0.008$); however, the mean aspect ratios of spermatozoa from the corpus and cauda were not different from each other (Steel-Dwass test, $P = 0.98$). In addition, the minor axis length of the ellipse was decreased by 3.1% from the caput to the cauda (Fig. S7B; two-tailed *t*-test, $P = 0.015$), whereas the major axis length was not significantly different between those groups (two-tailed *t*-test,

P = 0.58). Similar to the aspect ratio means, the coefficients of variation (i.e., SD normalized by mean) of the aspect ratios of B6N spermatozoa continuously decreased from the caput (8.4%) to the corpus (6.0%), to the cauda (5.3%). On the other hand, BDF1 epididymal sperm (caput, corpus, cauda) showed the same aspect ratio as B6N zona penetrated sperm (Fig. S10).

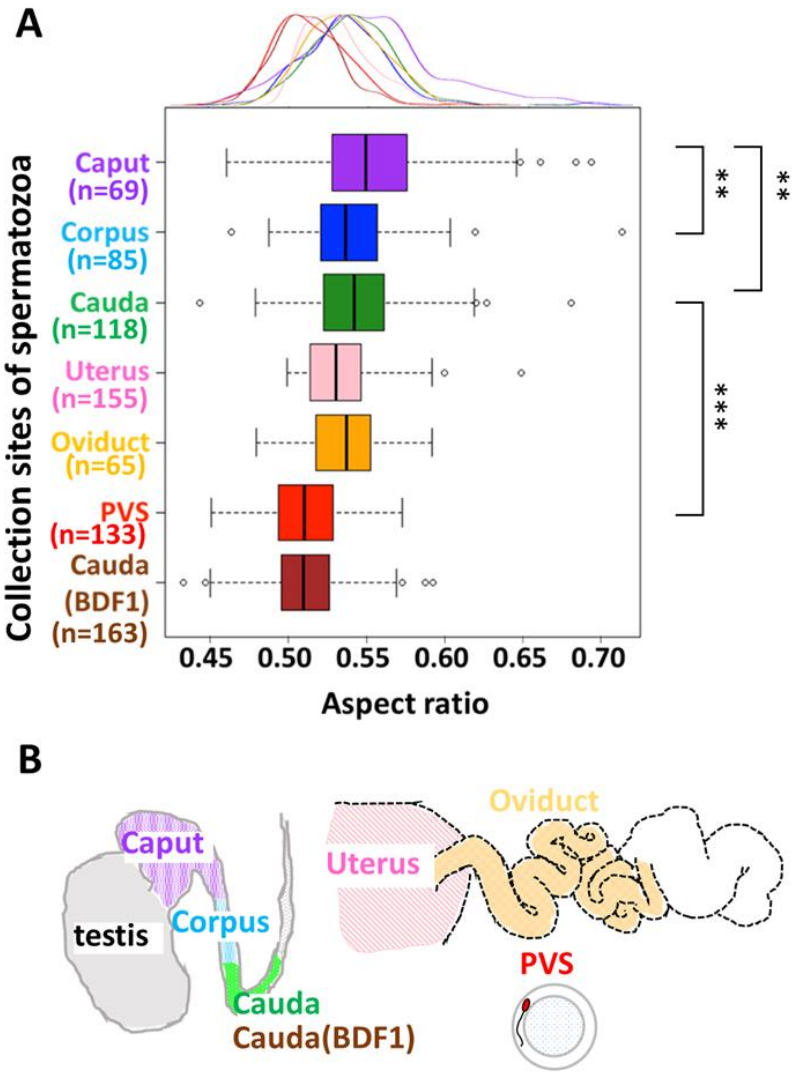

Figure. 2-4 The sperm head aspect ratio decreased during fertilization.

A box plot, with a corresponding density plot above the graph, depicts the sperm head aspect ratios, where the left/right hinge and the thick middle line represent the 25th/75th and 50th percentile, respectively. Spermatozoa were collected from the caput (purple), corpus (sky blue), and cauda (green) regions of the epididymis from B6N male mice (N = 3), or from the cauda epididymis from BDF1 male mice (brown; N = 3). B6N spermatozoa were also recovered from the uterus (pink) or oviducts (orange) of female mice (N = 3), and zona penetrated spermatozoa were recovered from the perivitelline space (PVS) of oocytes (red). The variance of the aspect ratio did not change during zona penetration (green and red; F-test, P = 0.12).

Finally, I also collected B6N spermatozoa from the uteri (n = 155) and the oviducts (n = 65; Fig. 2-4A) of females post-coitus, and I did not observe a difference in mean aspect ratio between these two locations (unpaired two-tailed *t*-test, $P = 0.22$). Moreover, to address whether the acrosome reaction [Dan 1952] causes the decreased aspect ratio of the zona-penetrated spermatozoa, I analyzed sperm morphology before and after the acrosome reaction by using transgenic Acr-EGFP (EGFP fused to the acrosome migrating signal; Fig. S1) mice and found that the acrosome reaction did not affect the aspect ratio in sperm nucleusTaken together, these data demonstrate that the aspect ratio of the sperm head did not change during entry of spermatozoa into the oviduct, but decreased during spermatozoon zona penetration.

Discussion

Possible mechanisms of the decreasing sperm head aspect ratio throughout the fertilization process

During spermatozoon maturation in the epididymides of B6N male mice, I found major morphological changes including decreases in head aspect ratios and minor axis lengths of the normal spermatozoa (Figs. 2-4, S7B, and S11). I found that the morphological change (decreases of aspect ratio) in the epididymis and during zona penetration are different (Fig. S11). The decrease in epididymis are likely due to structural changes that take place inside the sperm nucleus, which largely occupies the sperm head. During spermatogenesis in the testis, the DNA packaging histones are replaced by protamines, which more densely package every 50–60 kb of DNA into a toroid (donut) shape [Braun & Robert 2001]. In the caput, the toroids are subsequently cross-linked by disulfide (SS) bonds, resulting in further DNA compaction [Bedford &

Calvin 1974], which is consistent with our observed decrease in the sperm head minor axis length and aspect ratio in the caput-isolated spermatozoa. The aspect ratio of epididymal sperm of BDF1 was not different from B6N zona penetrated spermatozoa (Fig. S10). The DNA compaction is likely to be more advanced in BDF1. Thus, I hypothesize that the decreased aspect ratio in maturing spermatozoa from the epididymis is caused by the formation of SS bonds, which can be tested using dithiothreitol to reduce the SS bonds [Bedford & Calvin 1974] and must determine whether they are indeed responsible for these morphological changes in future.

In the female reproductive tract, the ratio of abnormal to normal spermatozoa was previously reported to decrease considerably at the utero-tubal junction (UTJ; junction of uterine and oviduct) [Krzanowska, 1974; Anne & Mary 1984]. Here, I showed that the normal spermatozoa isolated from the uteri and oviducts after coitus had similar sperm head aspect ratios (Fig. 2-4), suggesting that UTJ plays a role in eliminating the abnormal spermatozoa but not in altering normal sperm morphology. The decreases in sperm head aspect ratios that I observed during zona penetration (Fig. 2-4) could be due to the selection of a fractional sperm population [Utsuno et al., 2013; Beletti et al., 2005] or to the deformation of individual sperm. Sperm deformation has been attributed to the acrosome reaction [Dan 1952], which, in our case, I showed to be unlikely (Fig. S1), or to the mechanical force loaded at the time of the zona penetration. Thus, determining whether sperm subpopulation selection or mechanical deformation occurs during zona penetration, using methods such as time-lapse imaging and measuring the yield stress on the sperm head during zona penetration, will be important avenues for future examination.

Strategies for identifying the most fertile spermatozoa and implication for therapeutic applications

The correlation of sperm head morphology and fertilization ability (Figs. 2-2C and 2-4) suggests that spermatozoon morphology can be used as a strategy to screen mouse spermatozoa suitable for fertilization. Here, I showed that populations of spermatozoa with higher fertilization abilities (BDF1 cauda and B6N zona-penetrated in Fig. 2-4) had smaller aspect ratios, i.e., thinner heads, than other populations. The generality of this correlation should be further validated by applying our morphometry to zona-penetrated spermatozoa of other strains whose fertilization rates are well known, including DBA/2, BALB/c, 129S3/SvIm, and FVB/N (The Jackson laboratory., 2009). Moreover, even in spermatozoon populations with a large mean aspect ratio, there could be subpopulations with smaller aspect ratios and increased fertilization abilities. For instance, in our study, I observed a fraction of B6N cauda spermatozoa that morphologically overlapped with BDF1 cauda spermatozoa and B6N zona-penetrated spermatozoa, which have higher fertilization abilities (PC1 = 0.3–0.4 in Fig. 2-2C). Thus, evaluating whether these morphologically unique subpopulations will ultimately enable us to screen heterogeneous spermatozoon populations to identify good spermatozoa.

Applicability to human sperm

The correlation between aspect ratio and the success of fertilization in mice is consistent with a study showing that elongated sperm is more favorable for fertilization than rounded sperm [Ramón et al., 2014]. Human spermatozoa have been simply referred to be represented mainly by ellipses using Elliptic Fourier descriptors [Utsuno

et al., 2013]. Therefore, the present pipeline, which integrates geometric morphometrics with comparative morphology (Figs. 2-1 and 2-2), could be applied under the microscope in clinical laboratories. This pipeline would greatly facilitate and enhance current reproductive technologies in an objective, high-throughput manner.

Chapter3: Application of quantification procedure to human sperm

Abstract

Background.

In mouse spermatozoa, I established the pipeline which can compare the spermatozoa between high fertilizing ability and low fertilizing ability to find the morphological indicator that correlates with the success of fertilization, and showed that spermatozoa with higher fertilization rates have thinner nuclei. We have hypothesized that human sperm with high fertilization ability also has a low aspect ratio (i.e., thinner nuclei). In order to verify the hypothesis, I examined whether the combined method of EFDs and PCA can be applied to human sperm, and I compared the nuclear contour of normal human spermatozoa of fertile male and infertile male which have spermatozoa with normal motility and numbers..

Methods.

The features of human sperm head morphology were observed by using EFDs of sperm nuclear contour combined with PCA. I compared the spermatozoa of fertile males and infertile males instead of comparison between spermatozoa with high fertilization ratio and low fertilization ratio.

Results.

As a result of the principal component analysis of human sperm, the contribution ratios were PC1: 78.3%, PC2: 7.9%, PC3: 5.4%. Since principal components can explain the

human sperm head morphology in a few dimensions, it was confirmed that combined method of EFDs and PCA could be applied to human sperm. PC1 and aspect ratio showed a strong correlation. I have compared the spermatozoa between fertile and infertile. The spermatozoa of fertile males had significantly thinner head than spermatozoa of the infertile male.

Discussion.

I revealed that human spermatozoa of the fertile male had smaller aspect ratios, i.e., thinner nuclei. This result is consistent with the results of mouse experiments that spermatozoa with high fertilization rates have thinner nuclei. The aspect ratio can be applicable for choosing better sperm from many spermatozoa for fertilization (e.g., ICSI).

Materials & Method

Semen preparation by S. Kaneko (Tokyo dental college**)**

The pictures of spermatozoa were provided by S. Kaneko (Tokyo dental college). To compare the spermatozoa with the different fertilization ability, semen of infertility male (the failure to achieve a pregnancy after 24 months, N = 6) and male with children (fertile male, N = 3) were obtained by masturbation at Tokyo dental college Ichikawa general hospital. First, the photographs of spermatozoa were taken without fluorescence to confirm the position of the tail. Then, the spermatozoa were coated onto a glass slide (Matsunami Glass, Osaka, JP) and stained with 65 μM Hoechst 33342 (Life Technologies, Carlsbad, CA). The slides were viewed using an Olympus IX-70 fluorescence microscope with a 10× eyepiece and 100× objective lens (Numerical aperture is 1.4). The observation method of human spermatozoa is followed the experimental method of mice.

PCA

I analyzed the human sperm by PCA which previously described in “Materials and Methods” section of the chapter “Mouse Spermatozoa with Higher Fertilization Rates Have Thinner Nuclei”..

Statistics

I used Shapiro-Wilk test for checking normality, *F*-tests for checking homoscedasticity, *t*-tests were performed using custom R programs. A *P*-value > 0.05 was considered not significant (n.s.), whereas *P*-values < 0.05 (*), < 0.01 (**), and <

0.001 (***) were considered significant.

Result

Principal component analysis of human sperm morphology

The principal component analysis was applied to human sperm (N = 9, n = 983; Fig. 3-1). The contributions of the PC components were as follows; PC1: 78.3% PC2: 7.9% PC3: 5.4% PC4: 2.1% (PC1-4: 93.7%). To identify the PCs that correlate with fertilization ability, I focused on PC1, whose contribution rates were above 10% for normal human- sperm. The contribution ratio of the PC1 component was 28.5% larger than that in mice sperm (mouse PC1 = 49.8% in Table. 1). This result shows that the large part of the variation of human sperm morphology is explained by the PC1 component compared with that of the mouse. PC1 had strong correlation of aspect ratio with the aspect ratio (R^2 = 0.98). This was at least seven times higher than the correlation of PC1 with other coefficients of EFD (Table. 2). The result that the aspect ratio is strongly correlated with PC1 is consistent with that of mice sperm (Table. 2). This reduction of morphological information to low dimension indicated that EFDs and PCA could apply to human sperm.

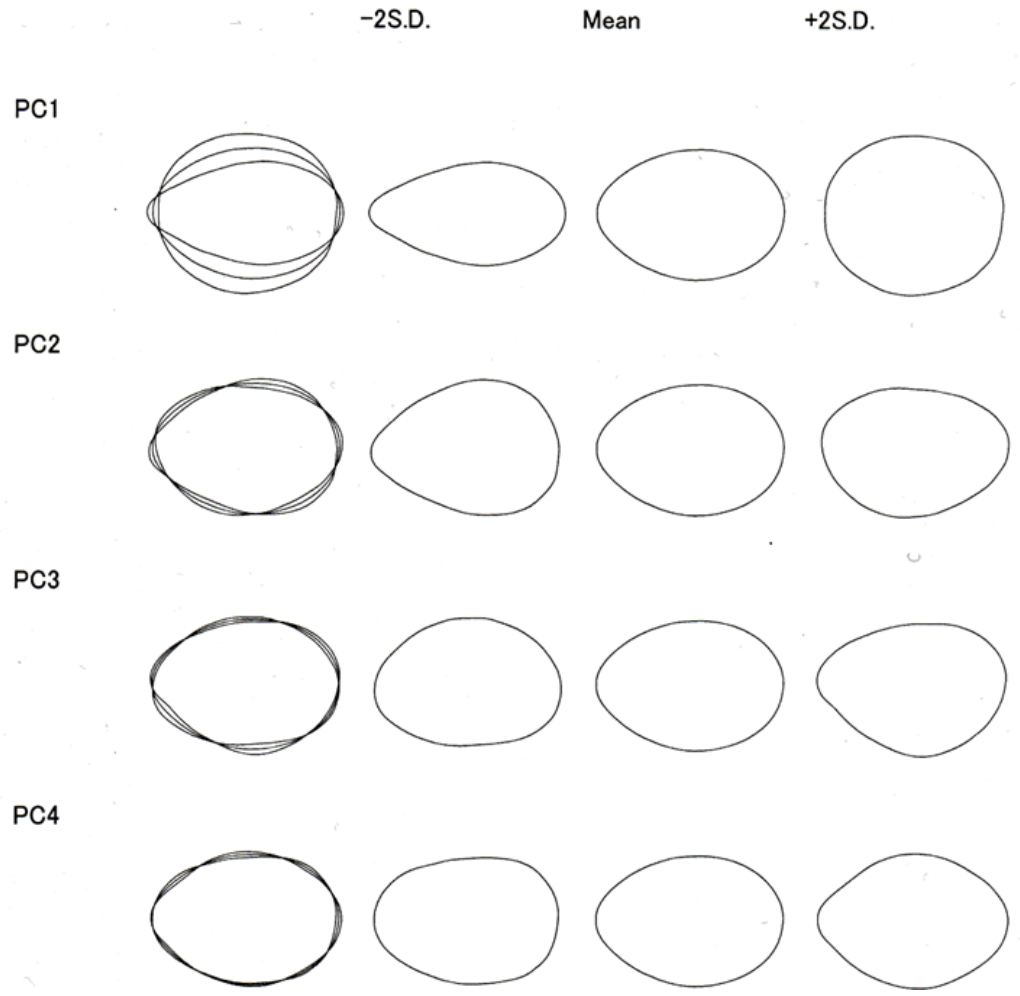

Figure.3-1 PCA result of human sperm morphology

From left to right, the overlapping, -2 standard deviation (SD), mean, and +2 SD sperm head contours of the first principal component (PC1-4) are shown from sperm head. The left side of the sperm head shows tail-side, and its right side of sperm head shows the acrosomal-side. PC1 showed ellipticity (the aspect ratio), and PC2 showed vertical anteroposterior asymmetry in human sperm. The features seen in PC3, PC4 were lateral asymmetry, angularity, respectively.

Contribution of spermatozoa		
	Human sperm (%)	Mouse sperm (%)
PC1	78.3	49.8
PC2	7.9	19.3
PC3	5.4	12.7
PC4	2.1	4.5

Table.1 The comparison of the contribution of spermatozoa between human and mouse. The red numbers show higher contribution than 10%.

	Factor lording			
	Human sperm		Mouse sperm	
1st	d1	0.98	d1	0.92
2nd	a3	0.14	c2	0.42
3rd	d3	0.02	d2	0.23
4th	d2	0.02	b4	0.18
5th	a2	0.01	b2	0.15

Table.2 The comparison of factor lording (correlation) of PC1 between human and mouse.

Comparison between Infertile and fertile male spermatozoa

In order to find the morphological indicator that correlates with the success of fertilization, I compared the sperm head morphology of infertile male with a fertile male in the principal component space. I found that higher PC1 was highlighted in infertile male sperm (Fig. 3-2A). Therefore, I compared the spermatozoa between fertile and infertile using aspect ratio mainly contributing PC1. First, I compare the histograms of aspect ratios and found that both of histograms of fertile and infertile had unimodal, symmetric distribution (Fig. 3-2B). In infertile males, spermatozoa with higher aspect ratio than 0.6 seem more abundant than fertile males. The spermatozoa of fertile males had a significantly thinner (smaller) aspect ratio in average than that of infertile male (Fig.3-2C, two-tailed t-test $P = 1.98 \times 10^{-7}$). Therefore, the aspect ratio is a morphological indicator that correlates with the success of fertilization.

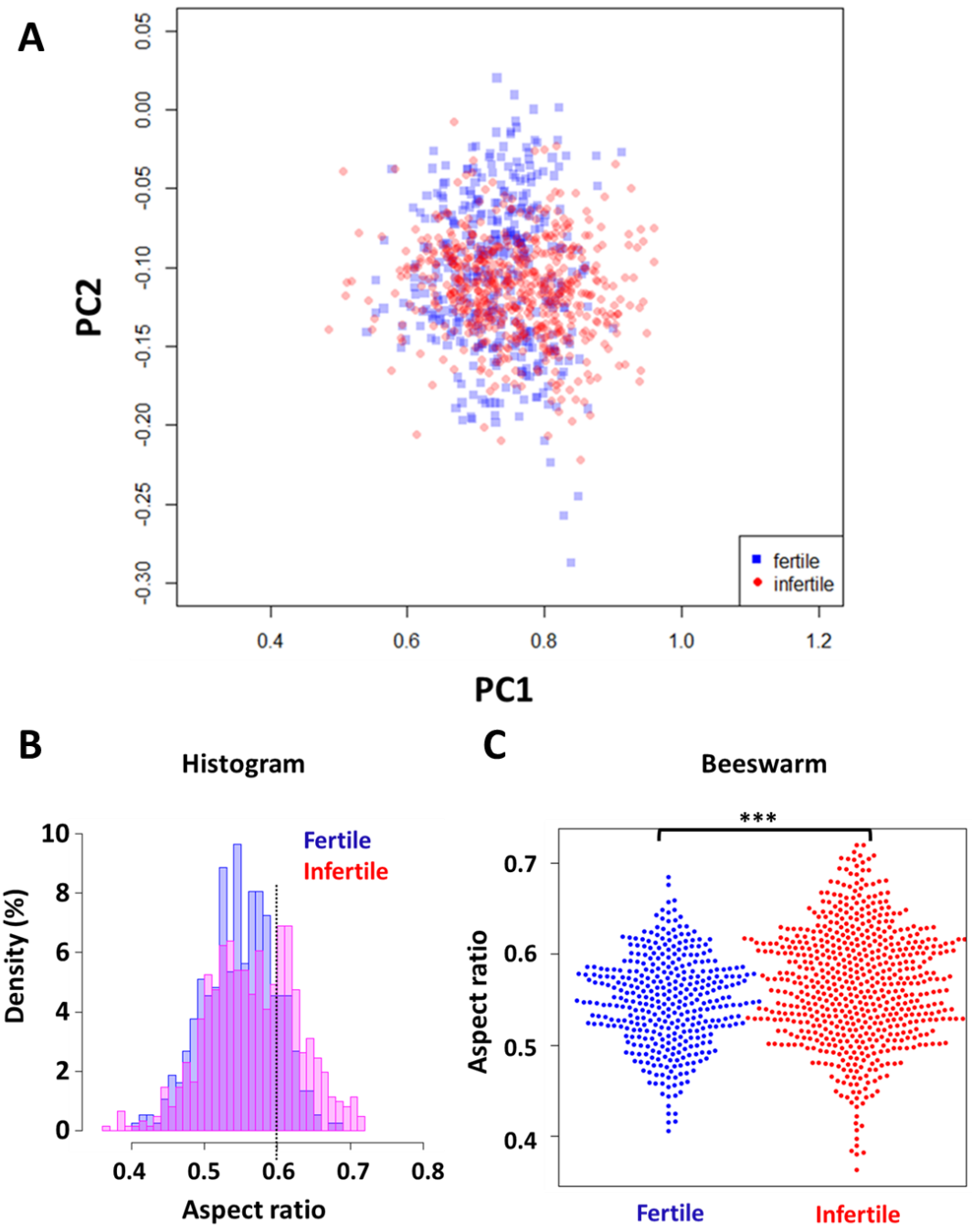

Figure.3-2 Fertile males have thinner nuclei.

A) Comparison of the spermatozoa between fertile and infertile male. The PCA analysis suggests that higher PC1 is highlighted in infertile spermatozoa. B) The ohistogram of spermatozoa of fertile/infertile males. As with PCA, higher (>0.6) aspect ratio is highlighted in infertile males. C) Beeswarm plot of spermatozoa of the fertile/infertile

male. Fertile males have thinner sperm head nucleus than infertile male (unpaired two-tailed *t*-test, P = 1.98 × 10-7).

Discussion

Using EFDs and PCA, I verified the hypothesis that human spermatozoa with high fertilizing ability ha thinner nuclei as with mice. Firstly, I found that the aspect ratio of human sperm head is strongly correlated with PC1, and fertile males have the spermatozoa withlower aspect ratio (i.e., thinner nuclei, Fig. 3-2B and C). This result is consistent with the study that shows the elongated spermatozoa has higher fertilization rate (Ramon et al., 2014). The recent study which showed thinner spermatozoa had higher fertilization rate (Nishikawa et al., 2017; higher pronucleus formation rate) is also consistent with our results that fertile males have more spermatozoa with lower aspect ratio (< 0.6) than infertile ones (Fig. 3-2B). Taken together, here I propose that the aspect ratio is the morphological indicator that correlates with the success of fertilization.

We can share the morphology of good human sperm with other researchers using the method I took in this study. The criteria of human normal sperm morphology are written in WHO lab manual: " A morphologically normal spermatozoon has an oval head and an acrosome covering 40%–70% of the head area. A normal spermatozoon has no neck, midpiece, tail abnormalities nor cytoplasmic droplets larger than 50% of the sperm head."), but it is difficult to ensure intra- and inter-laboratory reproducibility. As a method of sharing the morphology, there is a study that researchers tested whether they can separate normal and abnormal as Kruger did. However, this method could not be widely used. By combining EFDs and PCA, and determining the quantitative value in advance, we can easily share the morphology such as normal and abnormal and the sperm with high fertilizing ability.

As morphological indicators were common to human and mouse (Table. 3-3, Fig. 2-3, 3-2), to find where the morphology of human sperm changes using the indicator is a subject for future analysis. The results of measuring the morphology of mice sperm will serve as a reference for that (Table. 3). Mouse zona penetrated spermatozoa have thinner head (Fig. 2-4, Table. 3). Observation of human sperm penetration of the zona pellucida of human oocytes or humanized zona pellucida [Baibakov et al., 2012] of the mouse oocytes will be confirmed whether the thinner human spermatozoa can penetrate the zona pellucida. When the human zona penetrated sperm has thin sperm, it can be inferred that selection [Utsuno et al., 2013; Beletti et al., 2005] or deformation occurs during zona penetration as with mice, so that a good sperm can be selected or made. In mouse epididymis caput, the aspect ratio and its variability had higher than the sperm in epididymis corpus, cauda (Fig. 2-4, Table. 3). Observation of human epididymal sperm using excised epididymis of human (Yeung et al., 1993 use the dissected human epididymis which is epididymitis) will be confirmed whether the caput spermatozoa have the aspect ratio and its variability had higher than the sperm in epididymis corpus and cauda. When I observe the decrease of the aspect ratio of sperm in the human epididymis, I can assume that increased SS binding is occurring in epididymis as with the mouse. When I control this increasing of SS bond, it will be possible to make good sperm.

	Mouse	Human
Comparison between high and low fertilizing ability	BDF1 (>90%) has thinner head than B6N (60%). Fig. 2-3	Fertile males have the sperm with thinner head than infertile. Fig. 3-2
Comparison between closer and more distant to fertilization	Zona penetrated sperm has thinner head than ejaculated. Fig. 2-4	-
The morphology of epididymis	Caput sperm has thicker head than that of corpus/cauda. Fig. 2-4	-

Table. 3 The summary of our results.

Chapter4: Conclusion of the thesis

My motivation was to identify morphological indicators that correlate with the success of fertilization from normal spermatozoa. In order to find morphological indicator, I established a pipeline that can quantitatively compare the head morphology of spermatozoa of high fertilization ability with that of low fertilization ability, by combining method of EFDs with PCA. Moreover, I identified the quantitative indicators from the result of PCA. Using this pipeline, I showed that mice spermatozoa with high fertilization ratio have thinner nuclei, and mice spermatozoa in PVS also have thinner nuclei. In human sperm, fertile males have thinner head than infertile males. Therefore, the aspect ratio is the unique morphological indicator that correlates with the success of fertilization. Since the quantitative indicator has been heretofore absent, the criteria for selecting spermatozoa remain merely qualitative. The aspect ratio will be now a useful indicator for choosing better sperm for ICSI treatment.

In the present study, I quantified the morphology of sperm by combining EFDs and PCA, and compared the spermatozoa which have the different fertilizing ability, and I was able to differentiate the fertilizing ability with the aspect ratio. In this method, the contour shapes are quantified without losing information of morphology. But it takes time to analyze. As automation progresses in the future, the time to analyze will be reduced, and we will be able to find good sperm at the time we took the picture.

Few studies have analyzed the morphology by collecting zona penetrated spermatozoa. The oocytes of CD9 or Juno Knockout female mice show the defect of sperm-egg membrane fusion. Zona hardening does not occur unless fusion occurs, eggs allow multiple sperm invasion, so using these eggs, it will be able to collect zona penetrated sperm efficiently. Also, by using humanized zona pellucida of the mouse, it

will be possible to measure the morphology of zona penetrated human sperm.

I investigated the morphology of mouse spermatozoa in the male/female reproductive tract using an indicator in order to find out where the morphology of sperm are changed. I found that the spermatozoa in epididymis caput have higher aspect ratio than that of epididymis corpus and cauda. I showed that the morphology that correlates with the success of fertilization is changed during the sperm transition in the epididymis. Because it may be possible to make the sperm thinner to make a good sperm, it is worth investigating what mechanism causes the decrease of aspect ratio in epididymis. When the sperm penetrates the zona pellucida, the aspect ratio of spermatozoa decreased. This decrease would mean a mechanical deformation or selection. A recent prospective study that showed thinner human sperm have higher pronuclear formation ratio by ICSI suggests that the aspect ratio correlates with success fertilization regardless of deformation/selection. On the other hand, why thinner sperm has the high fertilizing ability is unknown, so it would be worth investigating.

- **References**

- **Bedford JM, Calvin HI. 1974**. The occurrence and possible functional significance of -SS- crosslinks in sperm heads, with particular reference to eutherian mammals. *Experimental Zoology* **188**: 137-155

- **Beletti ME, Da Fontoura Costa L, Viana MP. 2005**. A comparison of morphometric characteristics of sperm from fertile Bos taurus and Bos indicus bulls in Brazil. *Animal Reproduction Science* **85**: 105-116

- **Braun RE. 2001**. Packaging paternal chromosomes with protamine. *Nature Genetics* **28**: 10-12

- **Bruce WR, Furrer R, Wyrobek AJ. 1974**. Abnormalities in the shape of murine sperm after acute testicular X-irradiation. *Mutation Research/Fundamental and Molecular Mechanisms of Mutagenesis* **23**: 381-386

- **Coetzee K, Kruger TF, Lombard CJ. 1998**. Predictive value of normal sperm morphology: a structured literature review. *Human Reproduction Update* **4**: 73-82

- **Cohen J, McNaughton D. 1974**. Spermatozoa: the probable selection of a small population by the genital tract of the female rabbit. *Journal of Reproduction and Fertility* **39**: 297-310

- **Dadoune JP, Mayaux MJ, Guihard-Moscato ML. 1988**. Correlation between defects in chromatin condensation of human spermatozoa stained by aniline blue and semen characteristics. *Andrologia* **20**: 211-217

- **Dan JC. 1952**. Studies on the acrosome. I. Reaction to egg-water and other stimuli.*Biological Bulletin* **103**: 54-66

- **Devillard F, Metzler-Guillemain C, Pelletier R, DeRobertis C, Bergues U, Hennebicq S, Rousseaux S. 2002**. Polyploidy in large-headed sperm: FISH study of three cases. *Human Reproduction* **17**: 1292-1298

- **Eggert-Kruse W, Schwarz H, Rohr G, Demirakca T, Tilgen W, Runnebaum B.1996**. Sperm morphology assessment using strict criteria and male fertility under *in-vivo* conditions of conception. *Human Reproduction* **11**: 139-146

- **Fischer B, Adams CE. 1981**. Fertilization following mixed insemination with 'cervix-selected' and 'unselected' spermatozoa in the rabbit. *Journal of Reproduction and Fertility* **62**: 337-343

- **Fredricsson B, Björk G. 1977**. Morphology of postcoital spermatozoa in the cervical secretion and its clinical significance. *Fertility and Sterility* **28**: 841-845

- **Gandini L, Lombardo F, Paoli D, Caponecchia L, Familiari G, Verlengia C, Lenzi A. 2000**. Study of apoptotic DNA fragmentation in human spermatozoa. *Human Reproduction* **15**: 830-839

- **Garrett C, Liu DY, Clarke GN, Rushford DD, Baker HWG. 2003**. Automated semen analysis: 'zona pellucida preferred'sperm morphometry and straight-line velocity are related to pregnancy rate in subfertile couples. *Human Reproduction* **18**: 1643-1649

- **Inoue N, Satouh Y, Ikawa M, Okabe M, Yanagimachi R. 2011**. Acrosome-reacted mouse spermatozoa recovered from the perivitelline space can fertilize other

eggs.*Proceedings of the National Academy of Sciences of the United States of America* **108**: 20008-20011

- **Irvine DS. 1998**. Epidemiology and aetiology of male infertility. *Human Reproduction* **13**: 33-44
- **Iwata H, Ukai Y. 2002**. SHAPE: a computer program package for quantitative evaluation of biological shapes based on elliptic Fourier descriptors. *Journal of Heredity* **93**: 384-385
- **Jouannet P, Ducot B, Feneux D, Spira A. 1988**. Male factors and the likelihood of pregnancy in infertile couples. I. Study of sperm characteristics. *International Journal of Andrology* **11**: 379-394
- **Krzanowska H. 1974**. The passage of abnormal spermatozoa through the uterotubal junction of the mouse. *Journal of Reproduction and Fertility* **38**: 81-90
- **Kuhl FP, Giardina CR. 1982**. Elliptic Fourier features of a closed contour. *Computer Graphics and Image Processing* **18**: 236-258
- **Lee JD, Kamiguchi Y, Yanagimachi R. 1996**. Andrology: analysis of chromosome constitution of human spermatozoa with normal and aberrant head morphologies after injection into mouse oocytes. *Human Reproduction* **11**: 1942-1946
- **Liu DY, Baker HW. 1992**. Tests of human sperm function and fertilization *in vitro*.*Fertility and Sterility* **58**: 465-483
- **Liu DY, Garrett C, Baker HWG. 2003**. Low proportions of sperm can bind to the zona pellucida of human oocytes. *Human Reproduction* **18**: 2382-2389

- **Martin RH, Rademaker AW, Greene C, Ko E, Hoang T, Barclay L, Chernos J. 2003**. A comparison of the frequency of sperm chromosome abnormalities in men with mild, moderate, and severe oligozoospermia. *Biology of Reproduction* **69**: 535-539
- **Menkveld R, Franken DR, Kruger TF, Oehninger S, Hodgen GD. 1991**. Sperm selection capacity of the human zona pellucida. *Molecular Reproduction and Development* **30**: 346-352
- **Menkveld R, Stander FS, Kruger TF, Van Zyl JA. 1990**. The evaluation of morphological characteristics of human spermatozoa according to stricter criteria.*Human Reproduction* **5**: 586-592
- **Nakanishi T, Isotani A, Yamaguchi R, Ikawa M, Baba T, Suarez SS, Okabe M.200 4**. Selective passage through the uterotubal junction of sperm from a mixed population produced by chimeras of calmegin-knockout and wild-type male mice.*Biology of Reproduction* **71**: 959-965
- **Nestor A, Handel MA. 1984**. The transport of morphologically abnormal sperm in the female reproductive tract of mice. *Gamete Research* **10**: 119-125
- **Oka A, Aoto T, Totsuka Y, Takahashi R, Ueda M, Mita A, Sakurai-Yamatani S, Yamamoto H, Kuriki S, Takagi N. 2007**. Disruption of genetic interaction between two autosomal regions and the X chromosome causes reproductive isolation between mouse strains derived from different subspecies. *Genetics* **175**: 185-197

- **Ostermeier GC, Sargeant GA, Yandell TBS, Parrish JJ. 2001**. Measurement of sperm nuclear shape using Fourier harmonic amplitudes. *Journal of Andrology* **22**: 584-594
- **Otsu N. 1979**. A threshold selection method from gray-level histograms. *Automatica* **11**: 23-27
- **Palermo G, Joris H, Devroey P, Van Steirteghem AC. 1992**. Pregnancies after intracytoplasmic injection of single spermatozoon into an oocyte. *The Lancet* **340**: 17-18
- **Ramón M, Jiménez Rabadán P, García-Álvarez O, Maroto Morales A, Soler AJ, Fernández Santos MR, Garde JJ. 2014**. Understanding sperm heterogeneity: biological and practical implications. *Reproduction in Domestic Animals* **49**: 30-36
- **Severa L, Máchal L, Švábová L, Mamica O. 2010**. Evaluation of shape variability of stallion sperm heads by means of image analysis and Fourier descriptors. *Animal Reproduction Science* **119**: 50-55
- **Siddiquey AK, Cohen J. 1982**. *In-vitro* fertilization in the mouse and the relevance of different sperm/egg concentrations and volumes. *Journal of Reproduction and Fertility* **66**: 237-242
- **Sztein JM, Farley JS, Mobraaten LE. 2000**. *In vitro* fertilization with cryopreserved inbred mouse sperm. *Biology of Reproduction* **63**: 1774-1780
- **The Jackson laboratory**. **2009.** The Jackson Laboratory Handbook on Genetically Standardized Mice Six edition.

- **Toner JP, Mossad H, Grow DR, Morshedi M, Swanson RJ, Oehninger S. 1995**.Val ue of sperm morphology assessed by strict criteria for prediction of the outcome of artificial (intrauterine) insemination. *Andrologia* **27**: 143-148
- **Touré A, Szot M, Mahadevaiah SK, Rattigan Á, Ojarikre OA, Burgoyne PS. 2004**. A new deletion of the mouse Y chromosome long arm associated with the loss of Ssty expression, abnormal sperm development and sterility. *Genetics* **166**: 901-912
- **Toyoda Y, Yokoyama M, Hoshi T. 1971**. Studies on the fertilization of mouse eggs *in vitro*. *Japanese Journal of Animal Reproduction* **16**: 147-151
- **Utsuno H, Oka K, Yamamoto A, Shiozawa T. 2013**. Evaluation of sperm head shape at high magnification revealed correlation of sperm DNA fragmentation with aberrant head ellipticity and angularity. *Fertility and Sterility* **99**: 1573-1580
- **Van Waart J, Kruger TF, Lombard CJ, Ombelet W. 2001**. Predictive value of normal sperm morphology in intrauterine insemination (IUI): a structured literature review.*Human Reproduction Update* **7**: 495-500
- **Vilyana G, Dimitar P, Efrosini T, Todor C. 2017**. Relation between morphological defects in human spermatozoa and spontaneous abortions in patients undergoing ICSI. *Annuaire De L'Université De Sofia "St. Kliment Ohridski" Faculte De Biologie* **102**: 186-193
- **Watanabe T, Endo A. 1991**. Effects of selenium deficiency on sperm morphology and spermatocyte chromosomes in mice. *Mutation Research Letters* **262**: 93-99

- **World Health Organization (WHO). 2010**. *WHO laboratory manual for the examination of human semen and sperm-cervical mucus interaction* (5th edition). Cambridge: Cambridge University Press.
- **Wyrobek AJ, Bruce WR. 1975**. Chemical induction of sperm abnormalities in mice.*Proceedings of the National Academy of Sciences of the United States of America***72**: 4425-4429

Acknowledgement

We thank S. Nishioka and Y. Esaki (NPO for Biotechnology Research and Development) for preparing the zygotes; members of the theoretical biology laboratory for constructive criticisms; S.A.M. Young and T. Yao for critical reading of the manuscript.

List of authors publications in relation to the thesis

D Mashiko, M Ikawa, K Fujimoto., 2017, Mouse spermatozoa with higher fertilization rates have thinner nuclei, *PeerJ*

H Miyata, JM Castaneda, Y Fujihara, Z Yu…, D Mashiko (9th/21 authors), 2016, Genome engineering uncovers 54 evolutionarily conserved and testis-enriched genes that are not required for male fertility in mice, *Proceedings of the National Academy of Sciences*

H Miyata, Y Satouh, D Mashiko, M Muto, K Nozawa… , Sperm calcineurin inhibition prevents mouse fertility with implications for male contraceptive, *Science*, 2015

Supplemental Figures

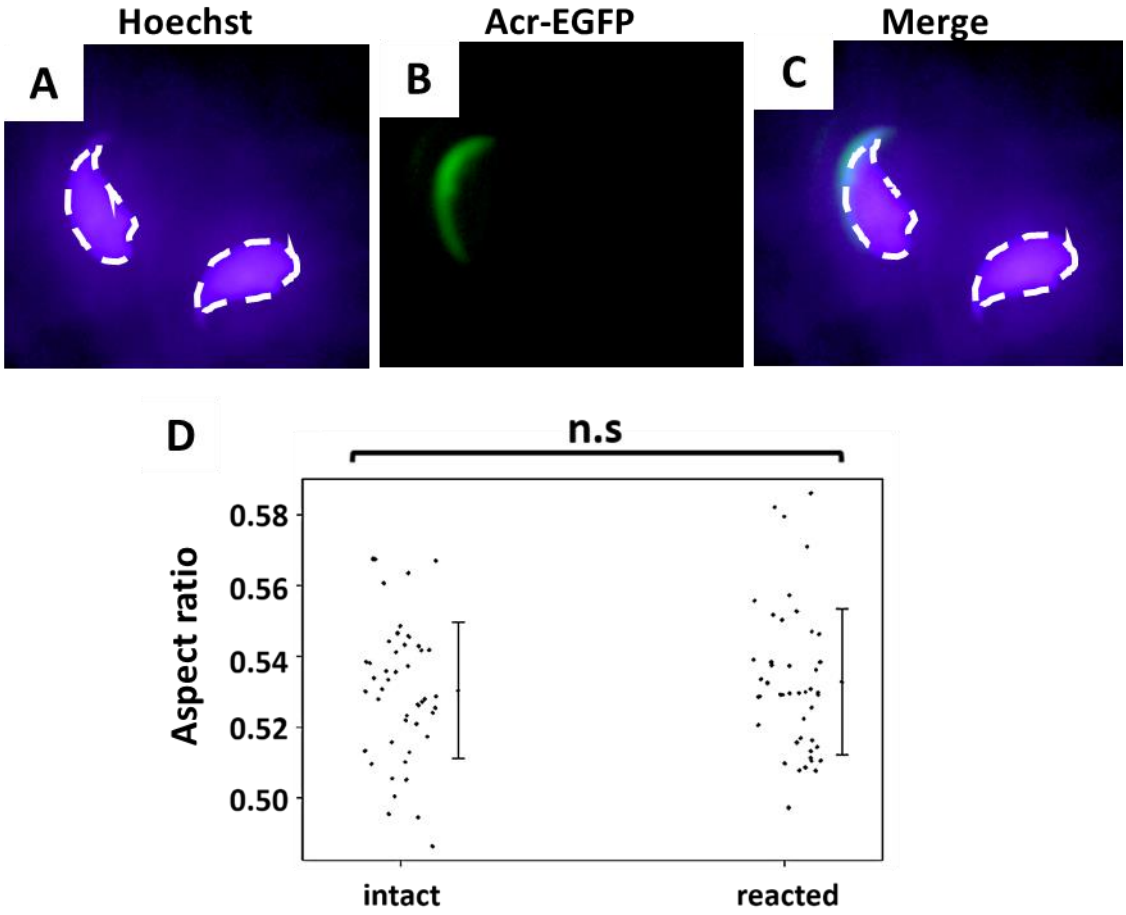

Figure S1. Acrosome reactions did not alter sperm nucleus morphology.

Images show the Hoechst-stained sperm nucleus **(A)**, the acrosome-reacted Acrosin-EGFP **(B)**, and the two images merged **(C)** following the spontaneous occurrence of an acrosome reaction after a 7-h incubation in TYH medium. In spermatozoa from Acrosin-EGFP mice [Nakanishi et al., 2004], the presence (left sperm in B and C) or absence (right sperm in B and C) of EGFP expression indicates intact or reacted acrosomes, respectively. **(D)** The aspect ratios of acrosome-intact (n = 44) and -reacted sperm (n = 46) were not significantly different (unpaired, two-tailed t-test; P = 0.12). The error bars indicate the standard deviations from the mean.

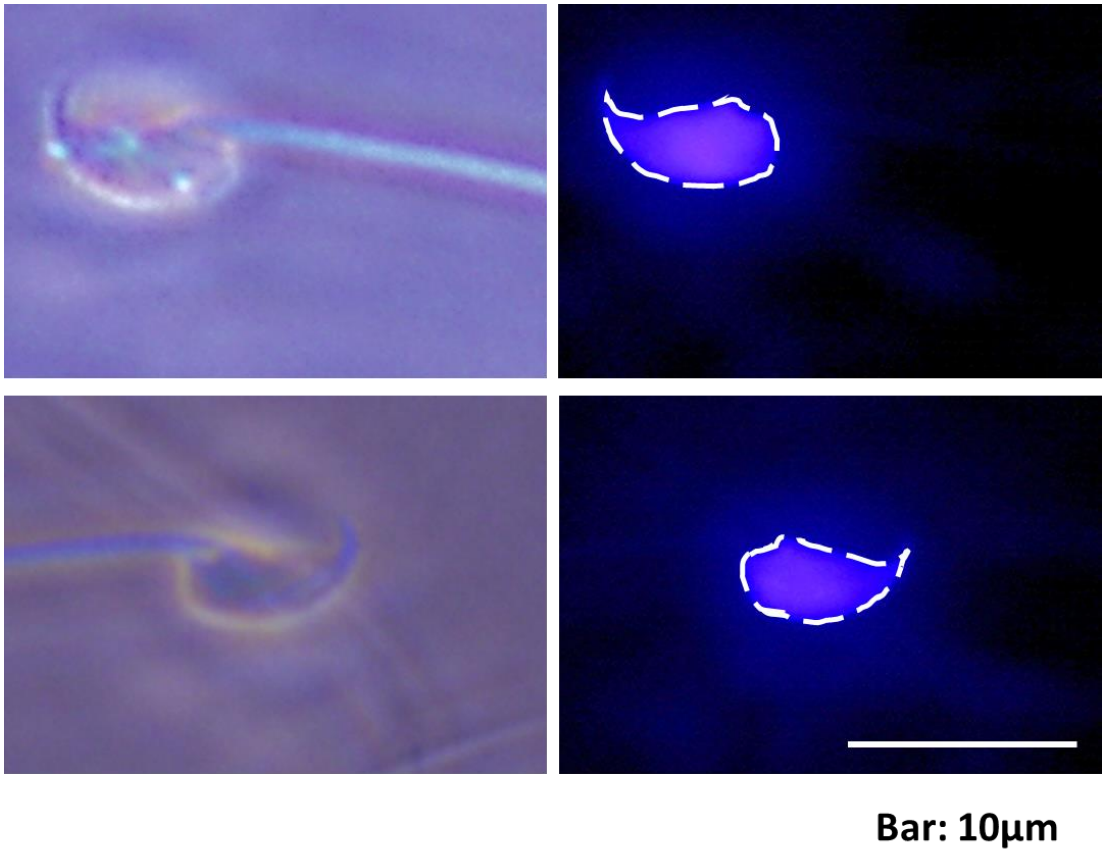

Figure S2. Hoechst-stained nuclei accurately represented the sperm head contour. Representative images show the head morphology (left panels) of two spermatozoa with Hoechst-stained nuclei (right panels). The contours of the sperm heads overlap completely with the Hoechst-stained nuclei. Nuclear staining makes measurement of morphology easier than observation by optical microscope.

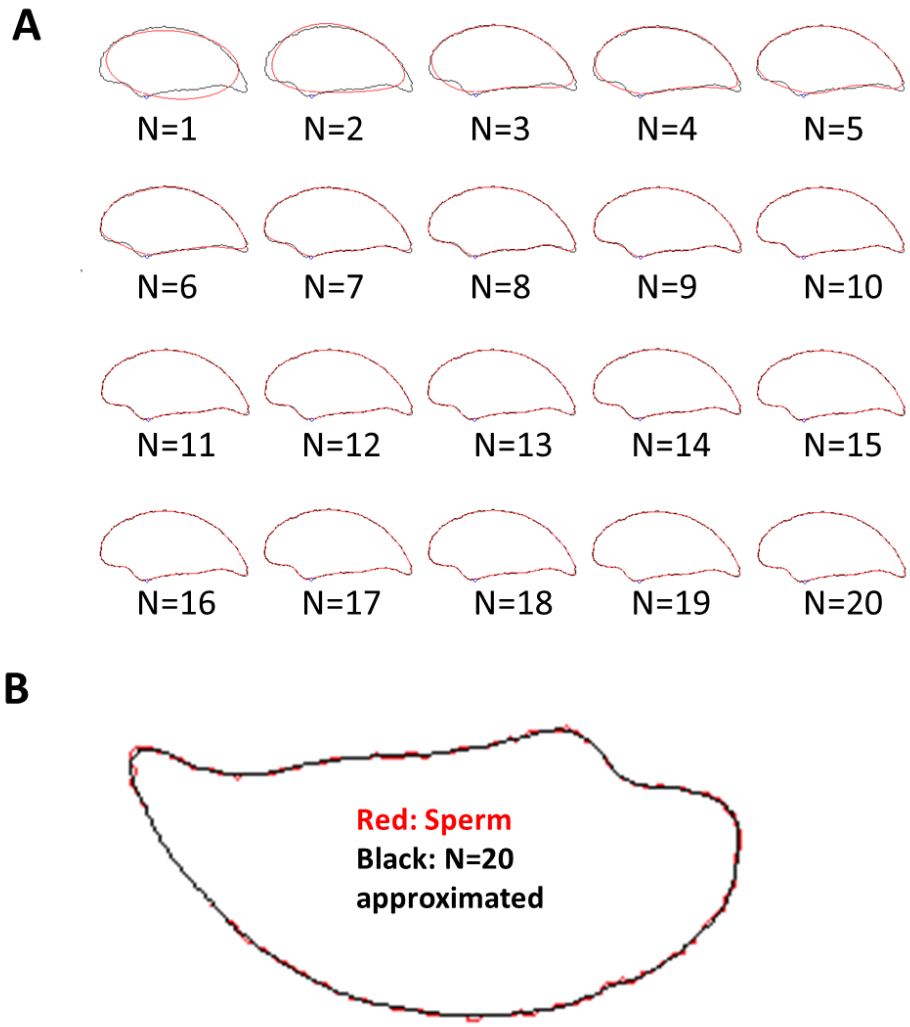

Figure S3. Elliptic Fourier descriptors accurately approximated the sperm head shape.

(A) *N* denotes the number of ellipses that were used to approximate the sperm head contour (black line; see also Eq. (1)). The approximated contour (red line) became more accurate as the *N* increased. **(B)** An enlarged view at *N* = 20 shows that the overlap of

red and black lines indicating a precise approximation.

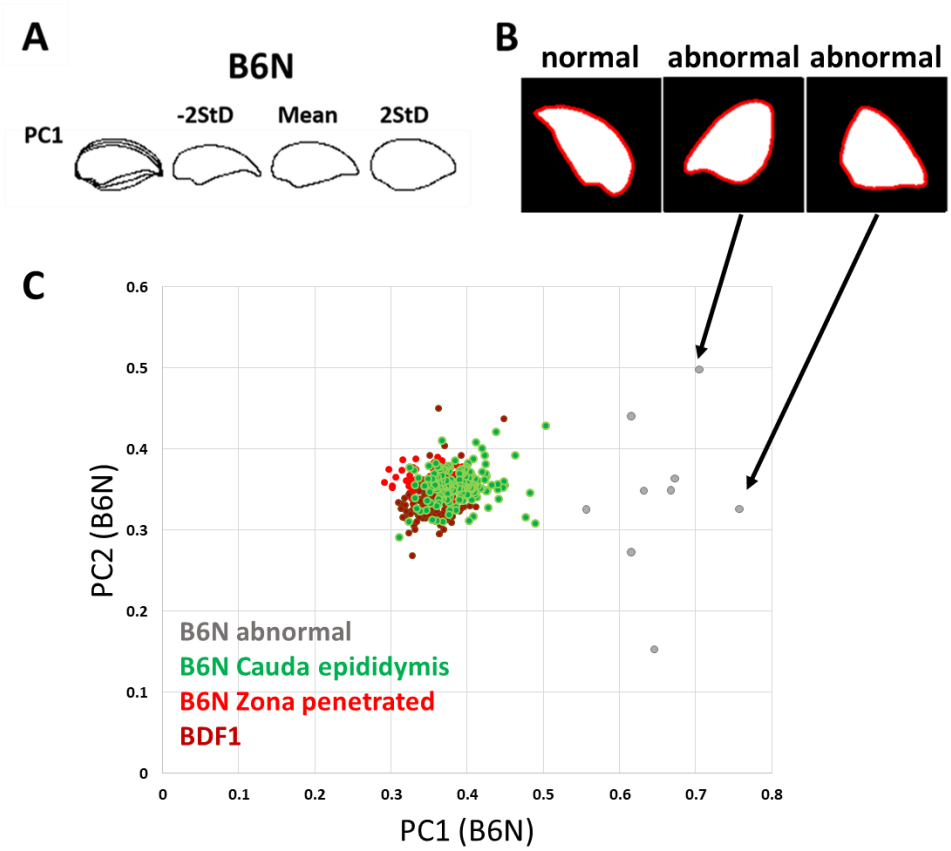

Figure S4. The inclusion of abnormal spermatozoa affected the principal component score.

(A) Principle component analysis (PCA) was performed of B6N cauda epididymis-isolated spermatozoa without exclusion of abnormal spermatozoa (n = 179). The standard deviation (SD) of the sperm head contours in the first principal component (PC1) are shown, and they appear higher than those without abnormal spermatozoa (Fig. 5A). **(B)** Images depict the contours of the normal and abnormal spermatozoa. The abnormal spermatozoa often lack the hook-shaped tip (arrows indicate their

corresponding PC score in panel (C). **(C)** Abnormal spermatozoa were distinguished from normal spermatozoa by PCA, and they had higher PC1 scores.

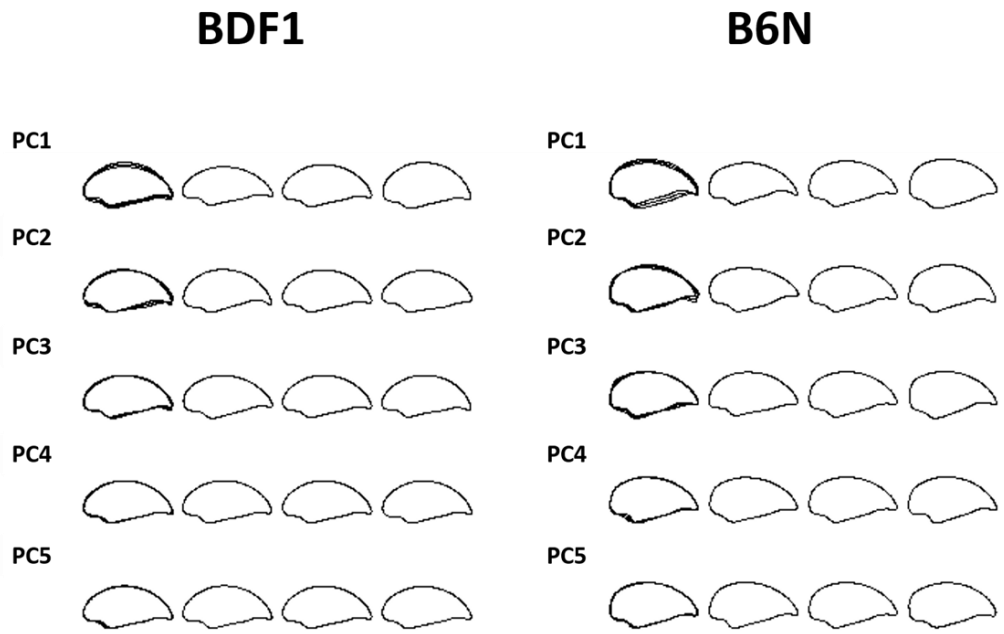

Figure S5. Morphological variation among mouse strains was reflected by multiple principal components.

From left to right, the overlapping, -2 standard deviation (SD), mean, and +2 SD sperm head contours of five principal components (PC1–5) are shown from BDF1 (left column) and B6N (right column) mouse epididymis-isolated spermatozoa.

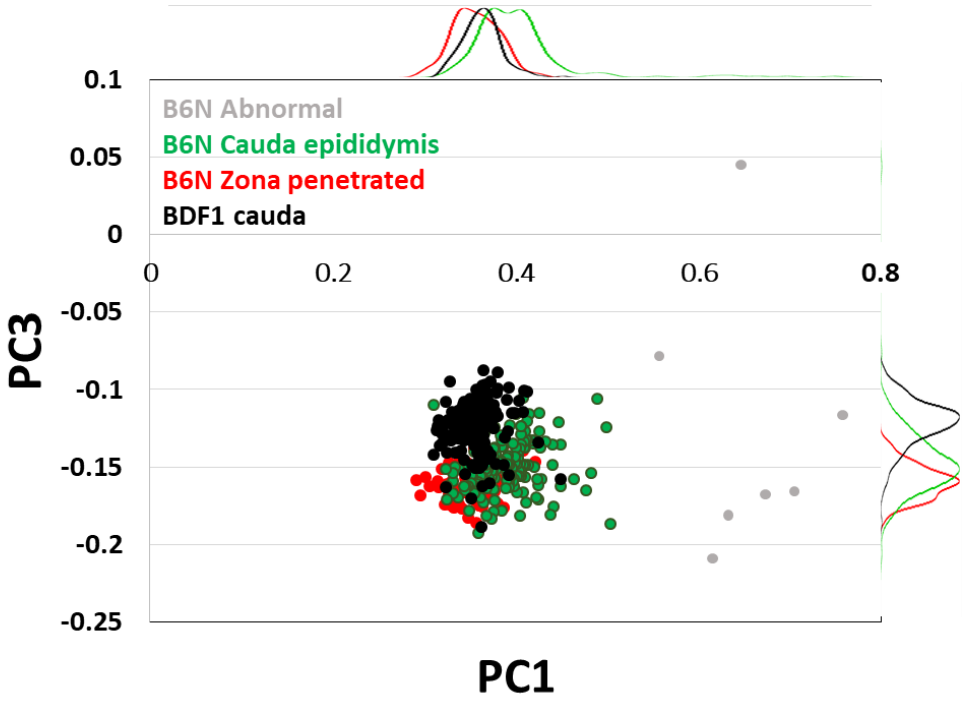

Figure S6. The third principal component distinguished spermatozoa among mouse strains but not fertilization stages.

A scatter plot and the associated density curves (outside of the x- and y-axis) of the first and third principal component (PC1 and PC3) scores of B6N zona-penetrated spermatozoa (red), and B6N (green) and BDF1 (black) cauda epididymis-isolated spermatozoa. Abnormal B6N cauda epididymis-isolated spermatozoa (gray) scores were also plotted on the PC1 and PC3 axes.

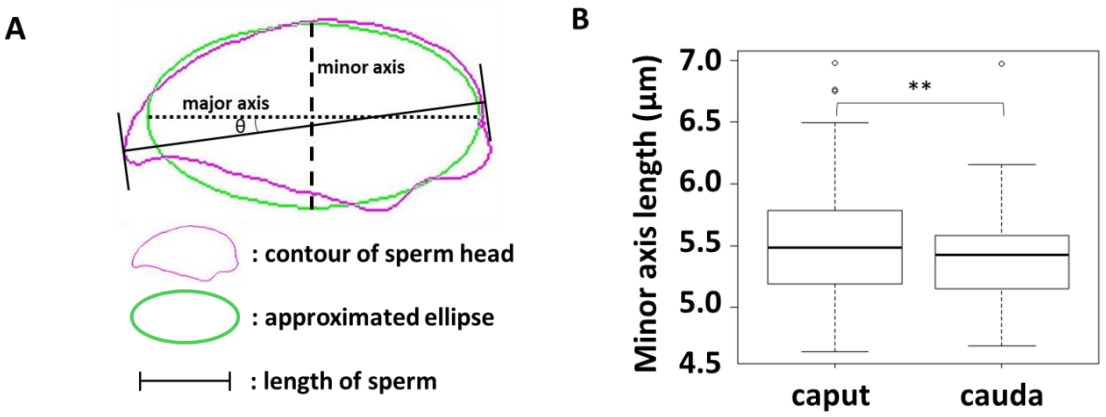

Figure S7. Sperm head measurements revealed alterations during sperm maturation.

(A) The longest part (solid black bar) of the sperm head contour (magenta line) was defined as the antero-posterior (AP) axis, which is consistent with a previous study [Utsuno et al., 2013]. The angle between the AP axis and major axis (dotted line) of the approximated ellipse (green line) of the sperm head (θ) ranged from 0.8 to 8.1 degrees among B6N cauda normal spermatozoa. The correlation coefficient between the AP axis (sperm head length) and major axis was 0.88 (n = 118, B6N cauda). We also measured the minor axis (dashed line), which is perpendicular to the major axis, to calculate the sperm head aspect ratio. **(B)** A comparison between B6N sperm heads of spermatozoa isolated from the caput and cauda regions of the epididymis revealed that the minor axis was significantly decreased (n = 69, caput; n = 118, cauda; one-tailed t-test, P = 0.015).

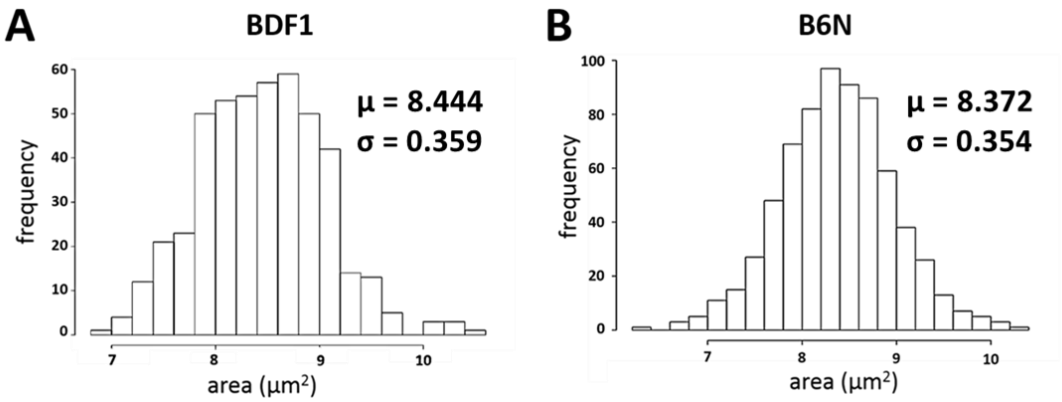

Figure S8. Sperm head areas were not different between BDF1 and B6N mouse strains.

Histograms show the range of sperm head areas of BDF1 (**A**, n = 687) and B6N (**B**, n = 465) spermatozoa. B6N spermatozoa showed a Gaussian distribution (Shapiro-Wilk normality test, P = 0.36), whereas BDF1 spermatozoa did not show a normal distribution (Shapiro-Wilk normality test, P = 0.02).

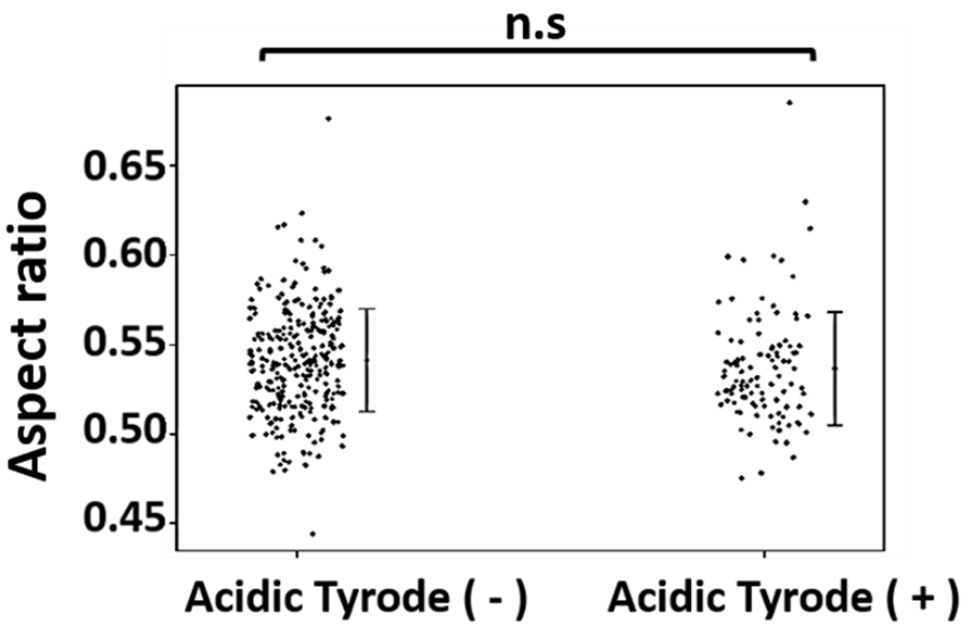

Figure S9. Treatment with acidic Tyrode's solution did not affect sperm nucleus shape.

The sperm head aspect ratios were not different following 2 h acidic Tyrode's solution treatment (+) (n = 298) and mock treatment (-) (n = 116) of B6N caudal spermatozoa (unpaired two-tailed t-test, P = 0.16). The error bars indicate the standard deviations from the mean.

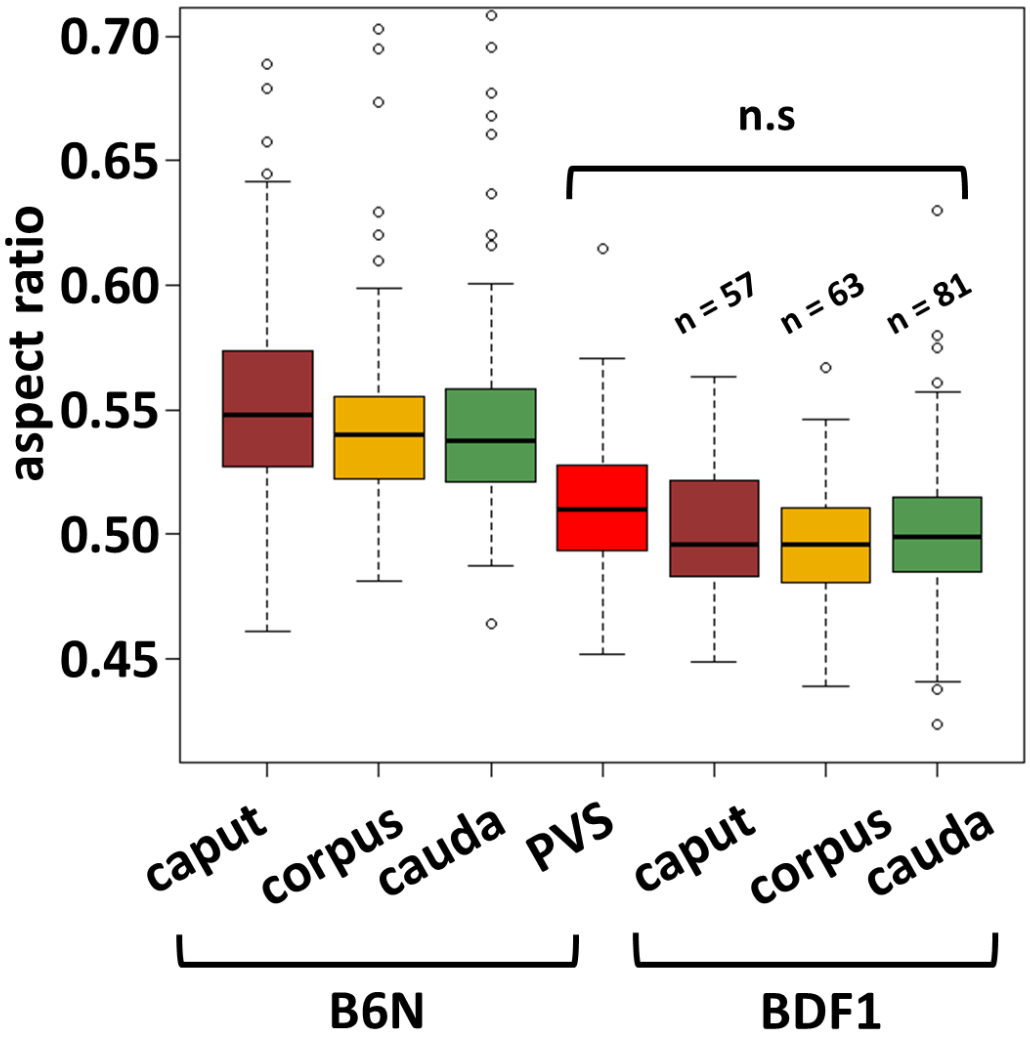

Figure S10 Epididymal spermatozoa of BDF1 and B6N do not show the difference.

The spermatozoa of B6N epididymis caput, corpus, cauda and spermatozoa in PVS are same as Fig.2-4. The number of BDF1 epididymal sperm is n=57, n=63, n=81, respectively (N = 5). There are not significantly difference between B6N PVS vs. BDF1 caput (one-tailed t-test, $P = 0.56$), BDF1 caput vs. BDF1 corpus (one-tailed t-test, $P = 0.83$), BDF1 corpus vs. BDF1 cauda (one-tailed t-test, $P = 0.72$)

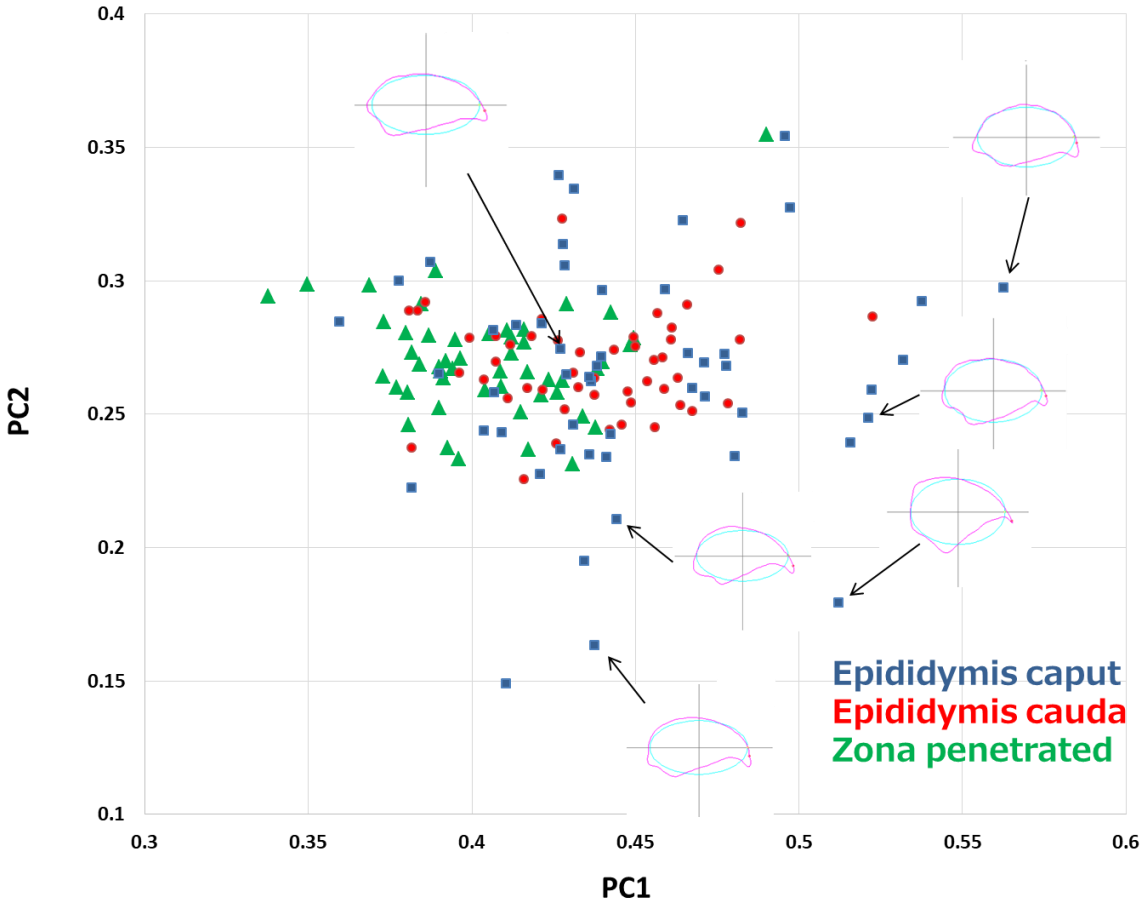

Figure S11. The decreases of the aspect ratio in male body and female body are different.

The spermatozoa of epididymis caput (blue), cauda (red), and zona penetrated (green) were plotted on morphospace of PCA. Caput spermatozoa showed higher PC1 and lower PC2. These morphology could not find in the spermatozoa of cauda epididymis. The comparison between cauda and zona penetrated spermatozoa shows the difference on PC1 but not PC2. Here, the decreases of aspect ratio in male body and female body have difference.